Spatiotemporal Variability of Precipitation, Modeled Soil Moisture, and Vegetation Greenness in North America within the Recent Observational Record

CHRISTOPHER L. CASTRO

Department of Atmospheric Sciences, The University of Arizona, Tucson, Arizona

ADRIANA B. BELTRÁN-PRZEKURAT AND ROGER A. PIELKE SR.

Cooperative Institute for Research in Environmental Sciences, Department of Atmospheric and Oceanic Sciences, University of Colorado, Boulder, Colorado

(Manuscript received 4 November 2008, in final form 20 May 2009)

ABSTRACT

Dominant spatiotemporal patterns of precipitation, modeled soil moisture, and vegetation are determined in North America within the recent observational record (late twentieth century onward). These data are from a gridded U.S.–Mexico precipitation product, retrospective long-term integrations of two land surface models, and satellite-derived vegetation greenness. The analysis procedure uses three statistical techniques. First, all the variables are normalized according to the standardized precipitation index procedure. Second, dominant patterns of spatiotemporal variability are determined using multitaper method–singular value decomposition for interannual and longer time scales. The dominant spatiotemporal patterns of precipitation generally conform to known and distinct Pacific SST forcing in the cool and warm seasons. Two specific time scales in precipitation at 9 and 6–7 yr correspond to significant variability in soil moisture and vegetation, respectively. The 9-yr signal is related to precipitation in late fall to early winter, whereas the 6–7-yr signal is related to earlysummer precipitation. Canonical correlation analysis is finally used to confirm that strong covariability between land surface variables and precipitation exists at these specific times of the year. Both signals are strongest in the central and western United States and are consistent with prior global modeling and paleoclimate studies that have investigated drought in North America.

1. Introduction

Land surface parameters considered at the atmosphere–land interface are soil temperature, snow cover, soil moisture, and vegetation. Soil moisture and vegetation are expected to be the dominant land surface effects. Their variability in space and time may affect the exchange of heat and moisture with the atmosphere. The role of the land surface in providing feedback to the atmosphere has been recognized on a wide range of scales, from the local and regional to global (e.g., Chase et al. 1996; Pielke 2001). The land surface, in turn, is affected by the forcing provided by the atmosphere, which is the subject of the present study. We emphasize

precipitation, as it is increasingly being used to characterize drought at multiple time scales through use of the standardized precipitation index (SPI; McKee et al. 1993). Precipitation, expressed in terms of SPI, has known significant variability in space and time. For temporal variability on the interannual to interdecadal time scale and spatial variability on the continental scale, the atmospheric forcing is related primarily to naturally occurring atmosphere–ocean interactions, such as El Niño–Southern Oscillation (ENSO).

This study investigates the statistical linkages between precipitation and land surface parameters in North America, specifically the contiguous United States and Mexico, within the recent observational record (since the late twentieth century). It is motivated by our prior work, which investigated the role of remote sea surface temperature (SST) forcing on climate variability in the warm season, using both observational analyses and regional climate modeling (Castro et al. 2001, 2007b). The dominant global modes of sea surface temperature

Corresponding author address: Dr. Christopher L. Castro, Department of Atmospheric Sciences, The University of Arizona, Physics and Atmospheric Sciences Bldg., Rm. 520, 1118 East Fourth Street, Tucson, AZ 85721-0081.
E-mail: castro@atmo.arizona.edu

anomalies (SSTAs), related to interannual and inter-decadal variability in the Pacific, affect the seasonal evolution of the North American monsoon system (henceforth NAMS) via remote forcing of the synoptic-scale circulation or teleconnections. The summer tele-connection patterns evolve in time and affect the onset of the North American monsoon in late June and early July. This conclusion is generally supported by other studies that have investigated the issue via statistical analyses of observations, including atmospheric rean-alyses (e.g., Mo and Paegle 2000; Hu and Feng 2002; Grantz et al. 2007).

Though statistically significant relationships between the NAMS and antecedent land surface conditions—such as snow cover and soil moisture—exist, Castro et al. (2001; 2007b) suggest these occur more as a passive re-sponse to the evolution of Pacific SST–associated tele-connection patterns through an annual cycle. Thus, in the core monsoon region (southwestern United States and northwest Mexico), a persistent condition of warm (cold) SST in the central and eastern equatorial Pacific would tend to favor a wet (dry) winter and a dry and delayed (wet and early) monsoon. By contrast, in the Great Plains, the precipitation anomaly signal associ-ated with Pacific SST variability is consistent throughout the whole year (i.e., consistently wet or dry for both warm and cool seasons). This spatial variability in warm-season precipitation on the regional scale is realized independently of the land surface forcing to the atmo-sphere, and this conclusion is generally supported by GCM studies (e.g., Schubert et al. 2002, 2004; Seager et al. 2005) and the paleoclimate record (e.g., Herweijer et al. 2007; Stahle et al. 2009). Considering individual years, it is known that soil moisture and vegetation can have strong responses to antecedent rainfall. For ex-ample, there is a rapid greening of vegetation and in-crease in soil moisture in the core monsoon region that occurs after the onset of the North American monsoon (Watts et al. 2007).

Statistical relationships between the land surface pa-rameters and atmospheric forcing on interannual and longer time scales exist in North America, and these generally agree with the aforementioned GCM and paleoclimate studies. Zhang and Mann (2005) inves-tigated coherent patterns of variation in Northern Hemisphere sea level pressure and conterminous U.S. summer drought for the twentieth century using the Palmer drought severity index (PDSI). Spatiotemporal patterns of variability on the interannual and bidecadal time scales are indicative of Pacific SST–associated cold- and warm-season influences on drought patterns. Soil moisture variability has also been analyzed directly from hydrologic models forced with long-term observed temperature and rainfall (e.g., Andreadis et al. 2005; Andreadis and Lettenmaier 2006). These studies find a multidecadal periodicity in droughts—with the most se-vere in the last century occurring in the 1930s, 1950s, and the late 1990s–early 2000s—as well a long-term decrease in drought intensity (with the southwestern United States being an exception). Leading modes of covari-ability of satellite-derived vegetation and precipitation also indicate a relationship with ocean–atmosphere anomalies (Lotsch et al. 2003), with the early 2000s drought being a period of below normal plant growth (Lotsch et al. 2005).

This study characterizes the spatiotemporal variabil-ity of modeled soil moisture and vegetation greenness in North America and its relationship to long-term varia-bility in precipitation forcing. The objectives of the study are 1) to derive the significant spatial patterns of pre-cipitation, modeled soil moisture, and vegetation green-ness variability and covariability on interannual and longer time scales; and 2) to examine the dependence of these patterns on seasonality and to determine the months in which the significant relationships exists and those months in which they do not. As will be shown, consideration of seasonality is of particular importance to the warm season because of the existence of the time-evolving teleconnections related to the NAMS de-scribed our own prior work. The paper is organized as follows: Section 2 describes the land surface and atmo-spheric data. Section 3 outlines the statistical analysis methods. Section 4 analyzes the dominant spatiotem-poral patterns in the three fields. Conclusions and ad-ditional discussion are given in section 5.

2. Datasets used for statistical analysis

a. Precipitation data

The precipitation data used are the 1° combined U.S.–Mexico daily precipitation product produced by the National Oceanic and Atmospheric Administration (NOAA) Climate Prediction Center (CPC; Higgins et al. 1996) and available from 1948 to the present, and we use these data through 2003 in this paper. These data can be accessed online via the CPC and the NOAA Earth System Research Laboratory. Precipitation data have been aggregated to the monthly time scale. Though the resolution of these data is relatively coarse, com-pared to other precipitation products that cover just the contiguous United States, they are used here primarily because there is data coverage in Mexico. However, the quality and amount of data in Mexico is generally poorer, which can affect spatial analyses (e.g., Castro et al. 2007b).

b. Modeled soil moisture

Primary modeled soil moisture data, given in terms of monthly volumetric soil water content averaged through the entire depth of the column, are obtained from a long-term, retrospective integration of the Variable Infiltration Capacity (VIC) land surface model, with observed atmospheric forcing for the period 1950–2000. These data were originally described in Maurer et al. (2002) and are available online through the Department of Hydrology at the University of Washington. These data cover the standard North American Land Data Assimilation System (NLDAS) domain, which includes all of the contiguous United States and part of northern Mexico, at ⅛° grid spacing. Similar soil moisture data from an extended integration of the Noah land surface model for the period 1948–98 (Fan et al. 2006) were also used to verify the results obtained using the VIC data. Soil moisture data are spatially degraded to 0.5° × 0.5° grid spacing before subsequent analysis, as this permitted the use of multitaper frequency domain–singular value decomposition (SVD) analysis (as described in the next section) with available computing resources. We emphasize that it is modeled soil moisture from retrospective long-term integrations of land surface models that is being analyzed. There are processes that affect soil moisture within all land surface models that are very difficult to represent or not captured at all, such as snowpack and snowmelt processes and dynamic vegetation. Analysis of two land surface models with different physical representations of land surface processes gives greater confidence that significant patterns, not artifacts of the individual models, are being considered.

c. NDVI data

Vegetation status was analyzed using the Global Inventory Modeling and Mapping Studies (GIMMS) satellite drift–corrected and NOAA-16-incorporated normalized difference vegetation index (NDVI) dataset (Pinzón 2002; Pinzón et al. 2004; Tucker et al. 2005). Corrections performed to this dataset account for volcanic aerosols due to major eruptions in 1982 and 1991, sensor degradation, and satellite drift. NDVI is the ratio of the difference between the Advanced Very High Resolution Radiometer (AVHRR) reflectance in the near-infrared and visible bands and the sum of these two bands; it ranges between −1 and +1. Green leaves have a higher reflectance in the near-infrared band than in the visible band as a result of stronger chlorophyll absorption in the visible band. Therefore, NDVI increases with green leaf vegetation density: nonvegetated surfaces have low NDVI values of around 0.2 and dense vegetated surfaces have a value higher than 0.7. Bimonthly

maximum value composite of GIMMS NDVI is available globally for an 8 km × 8 km footprint from July 1981 to the present. Here we use the period 1981–2003. These data were regridded to the Regional Atmospheric Modeling System (RAMS) model grid used in Castro et al. (2007a). Daily NDVI values were obtained by linear interpolation.

3. Statistical analysis procedures

a. Variable normalization by the SPI technique

The SPI expresses the degree of dryness or wetness for a given location as a standard normal variable. It is increasingly gaining favor as a primary indicator of drought in climate monitoring (e.g., Heim 2002). There are two principal motivations for using the SPI in lieu of raw precipitation. First, it accounts for the fact that precipitation amounts for any given length of record typically follow a gamma distribution, not a normal distribution. This is especially the case for the dry climates of the interior western United States, where the index was originally developed. Second, it can be computed for a variety of time scales, typically from 1 to 24 months, to characterize short- or long-term drought conditions. In this study, the 1–6-month SPI is considered, using the CPC U.S.–Mexico precipitation data. Results are shown in section 4 for the 1- and 3-month SPI. The SPI is computed according to the original methodology in McKee et al. (1993) and Edwards and McKee (1997).

The same methodology used to compute the SPI is also applied to soil moisture and NDVI. Although there are few examples of application of the SPI analysis technique to other variables, it was recently completed for streamflow in Arizona (Schonauer 2007). A gamma distribution provides a more robust description of the distribution of land surface parameters because these are driven, in great part, by precipitation. It is also inappropriate to consider the raw averages and standard deviations of both soil moisture and vegetation greenness in the investigation of large-scale spatiotemporal variability because they can vary greatly in space because of rapid shifts in bioclimatic regimes associated with complex terrain. Unlike precipitation, a standardized index measure for a given land surface variable—soil moisture or NDVI—is computed only on a monthly time scale, not multiple months.

b. MTM–SVD analysis

Once the precipitation and land surface variables have been normalized using the SPI technique, we want to determine their dominant spatiotemporal patterns of
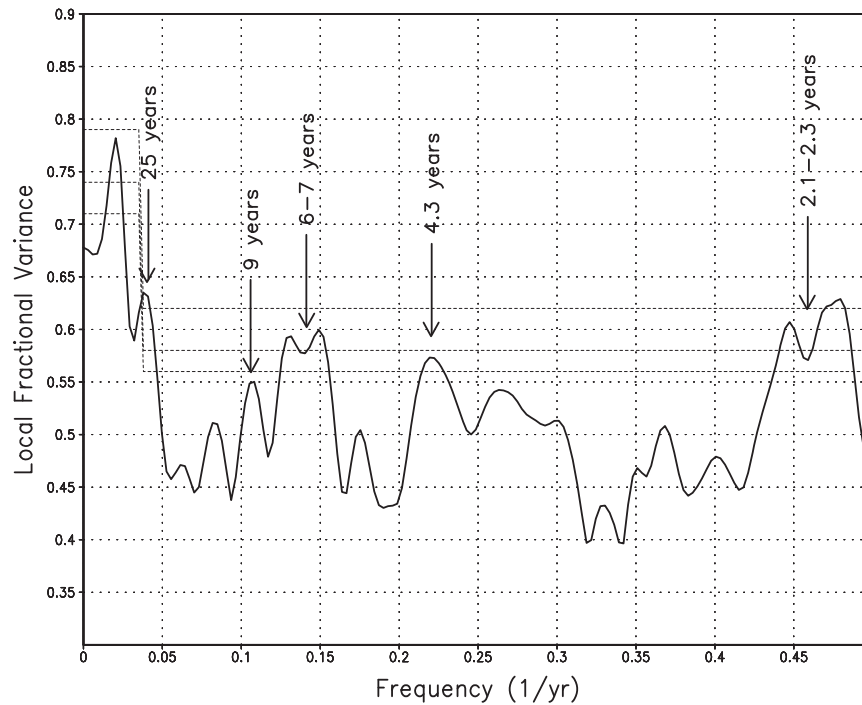
FIG. 1. Principal eigenmode LFV spectrum for the 3-month SPI computed from the CPC U.S.–Mexico precipitation dataset (1948–2003). Dashed lines indicate statistical significance at the 90%, 95%, and 99% confidence intervals. Significant spectral peaks and their appropriate corresponding time scale are indicated.

variability. A multitaper method (MTM) frequency domain–SVD analysis allows for the detection and reconstruction of quasi-oscillatory spatiotemporal signals that exhibit episodes of spatially correlated behavior, and it has demonstrated utility in a wide variety of geophysical applications (Rajagopalan et al. 1998). It produces 1) a local fractional variance (LFV) spectrum of the principal eigenmode; 2) statistical confidence intervals for the LFV spectrum; and 3) reconstructed patterns corresponding to the significant time-varying modes, referenced to a particular grid point within the domain. The specific details and references for the method are included in the appendix. We previously used this technique in Castro et al. (2007b) to characterize global SSTA patterns, and these results largely agreed with the dominant modes of a rotated EOF analysis. Typically when MTM–SVD has been used in climate research applications, as is the case here, of principal interest are low-frequency oscillations on the interannual to multidecadal time scales. Therefore, variability at a frequency greater than 0.5 yr^{-1} is not shown on the LFV spectrum.

MTM–SVD analysis is applied to the each of the normalized datasets in the following way: The analysis is first applied to the total dataset. For example, using a period of 50 yr, the analysis would be performed on

600 maps of monthly data. This provides a "first cut" analysis to reveal any statistically significant spatiotemporal signals. Then, to reveal which time(s) of year drives a particular signal in the LFV spectrum, the analysis is applied only for one month per year. So, following on the previous example, 12 new analyses would be performed on 50 maps, generating an individual LFV spectrum per month. Performing the analysis in this way implicitly emphasizes the existence of time-evolving teleconnections, which affect North American climate over very "narrow" windows of time (e.g., Figs. 5 and 6 of Castro et al. 2007b).

Reconstructed spatial patterns corresponding to the significant time-varying modes are then obtained for the SPI. In accordance with Rajagopalan et al. (1998), the pattern reconstruction map is shown as a vector plot referenced to a user-defined reference grid point within the analysis domain. The length of the vector gives the magnitude of the normalized anomaly, which projects into the given significant frequency band, and the vector direction represents the degree of phasing with respect to the reference grid point. A grid point completely in phase with the reference grid point would show a vector pointed directly eastward. In the plots shown, the in-phase component is also shaded, as in Fig. 1 of Castro et al. (2007b). The specific reference grid point we chose
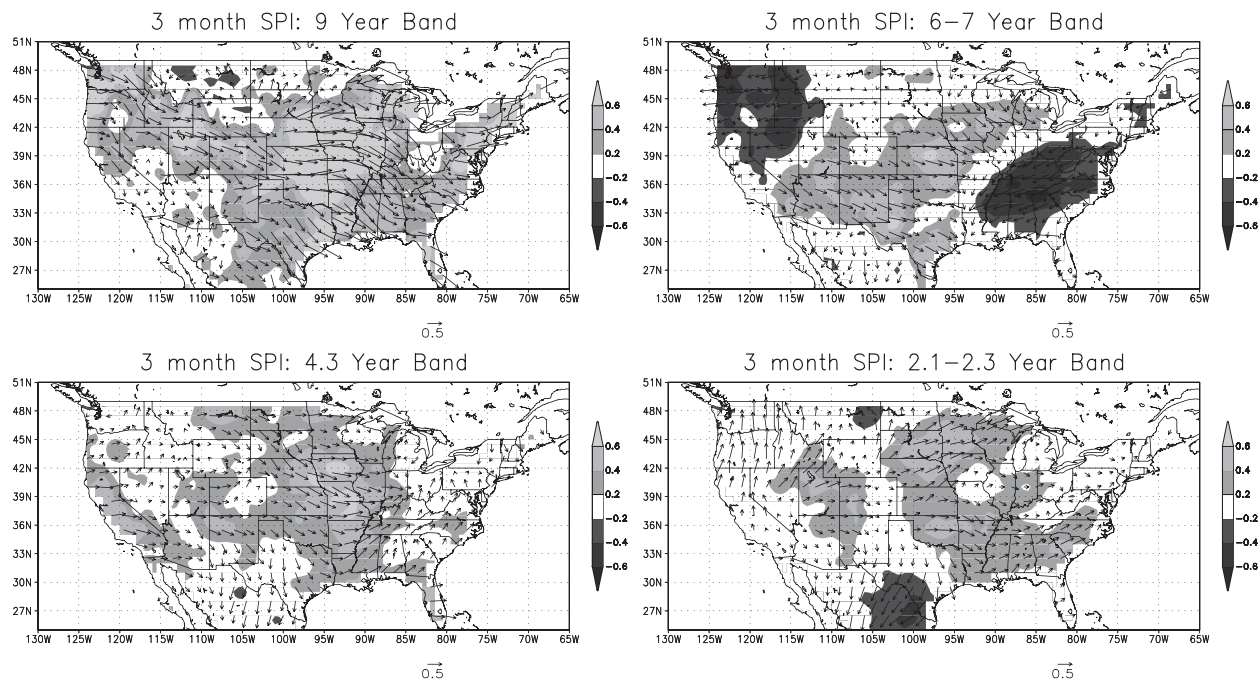
FIG. 2. Reconstructed spatial pattern vectors corresponding to significant spectral peaks in the 3-month SPI from Fig. 1, referenced to a grid point in the central United States (36°N, 97.5°W). Reconstruction of 25-yr peak omitted, as stated in the text. In-phase component shaded with scaling indicated by the grayscale bar. Vector length is 0.5.

is located in the central United States (approximately 36°N, 97.5°W), as this is an area where there is a consistent and statistically significant relationship of precipitation with Pacific SSTs throughout the year (Castro et al. 2001).

For (standardized) modeled soil moisture and NDVI, the reconstructed spatial patterns are shown a bit differently. First, the reconstructed time series corresponding to the significant frequency band of the standardized data is constructed for all grid points in the analysis domain. These data are regressed on the original time series. Then, the regression coefficient is divided by the average value of the original variable to produce the percentage difference from climatology. This quantity is then displayed with phasing information as a vector plot. The advantage to displaying the reconstructed spatial patterns in this way, rather than the direct result from the analysis of standardized variables as with the SPI, is that areas in which significant low-frequency signals in land surface parameters are largest with respect to their climatological values are emphasized.

c. Canonical correlation analysis

Once the dominant spatiotemporal patterns of precipitation and land surface variables are determined by MTM–SVD, their covariability is assessed using CCA

for the specific periods of the year, with the most statistically significant signals as indicated by LFV spectra. The specific methodology used for CCA follows Barnett and Preisendorfer (1987), as summarized by D. Hartmann in online course notes (available online at http://www.atmos. washington.edu/~dennis/552_Notes_ftp.html). First, principal component (PC) analyses are performed on two spatial fields with the same time dimension—namely, the SPI and either soil moisture or vegetation greenness. SVD is then performed on a covariance matrix of truncated principal components. The canonical correlation spatial pattern maps are computed by correlating the original data with its singular vectors, or expansion coefficient time series, for each data field obtained by SVD. The singular values obtained by SVD yield the canonical correlations. In displaying the spatial patterns of the canonical correlations, we show the homogeneous correlation maps of the first canonical vector only. It is not clear how to determine how many principal components to retain in CCA using the Barnett and Preisendorfer method. For our analysis, the canonical vectors are considered to represent physically reasonable patterns of covariability if the first canonical correlation is approximately 0.4–0.5, the spatial patterns in the homogeneous correlation maps resemble the dominant spatiotemporal pattern of the individual variables, and the homogeneous correlation maps are fairly invariant
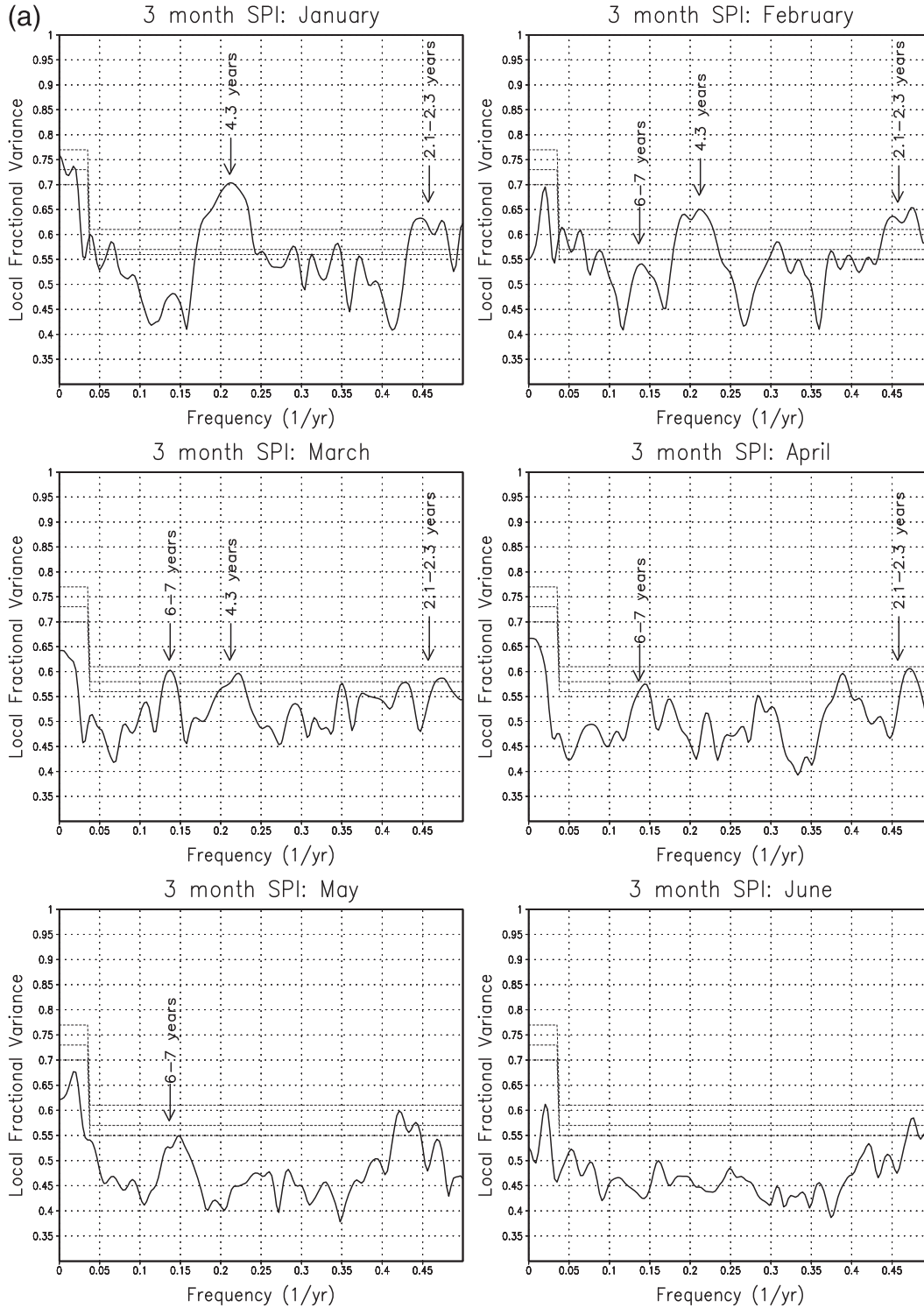
(a)

FIG. 3. Same as Fig. 1 but for the 3-month SPI of individual months. Only statistically significant peaks corresponding to the entire dataset in Fig. 1 are indicated.
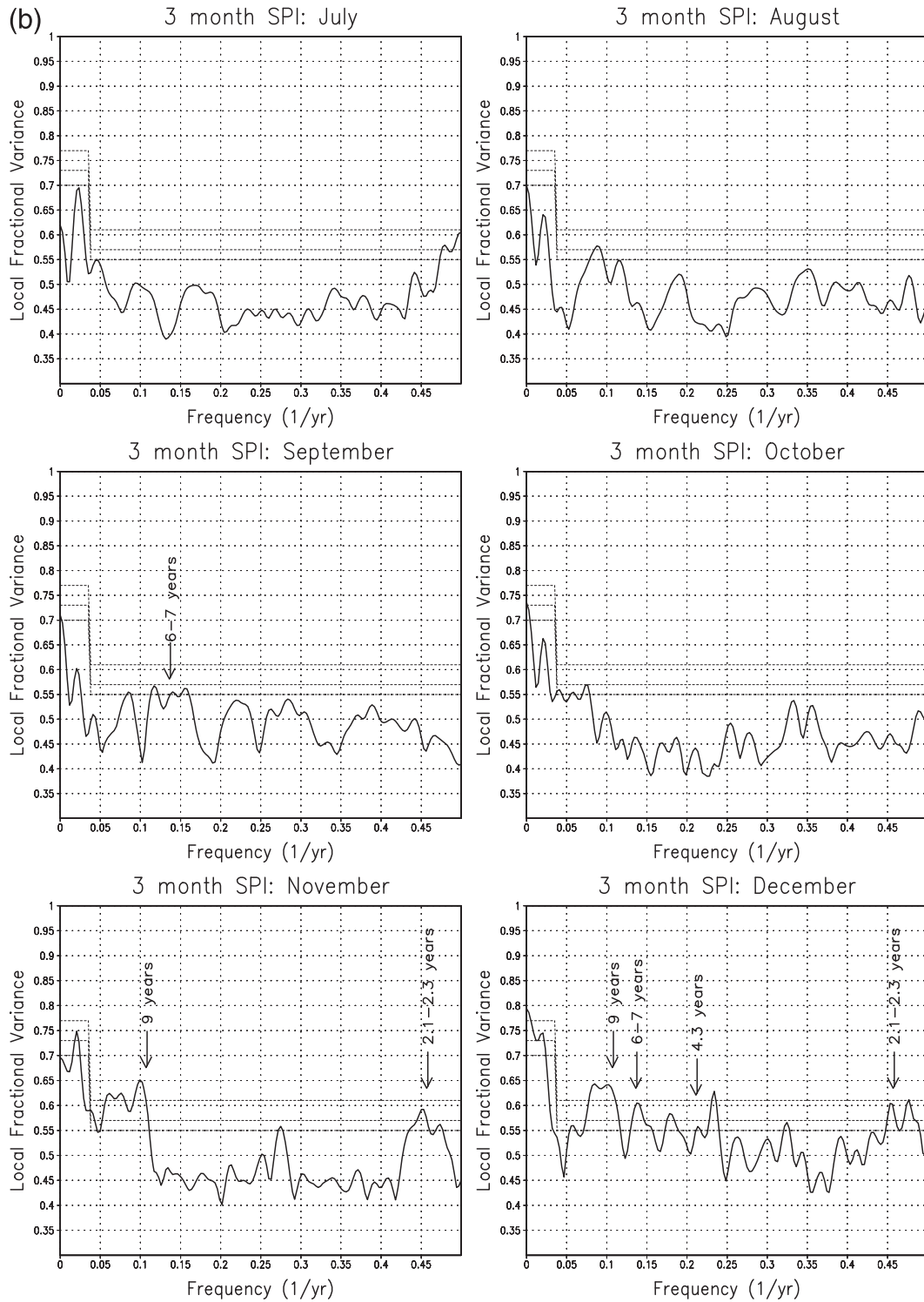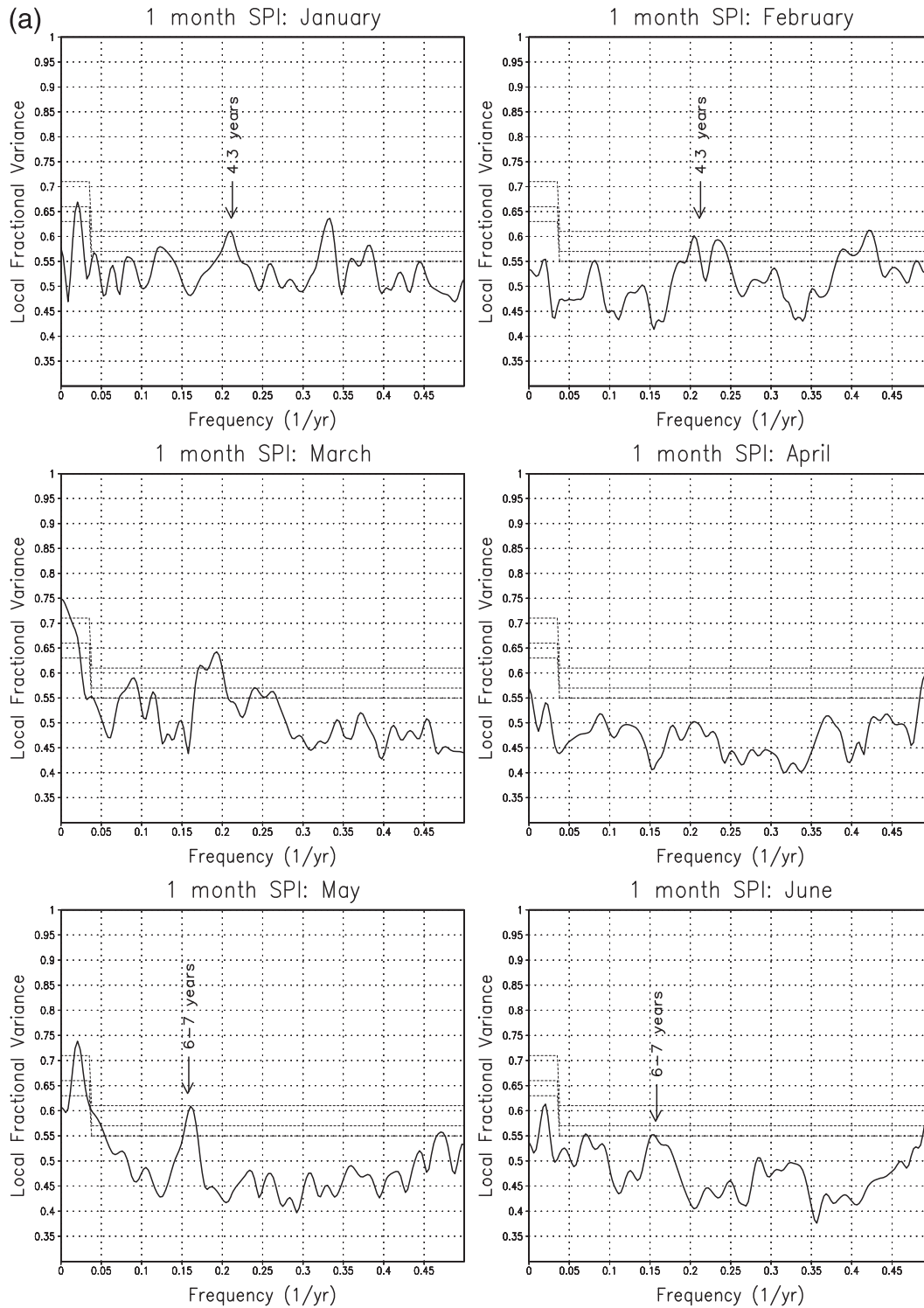
FIG. 3. (*Continued*)

FIG. 4. Same as Fig. 3 but for the 1-month SPI of individual months.
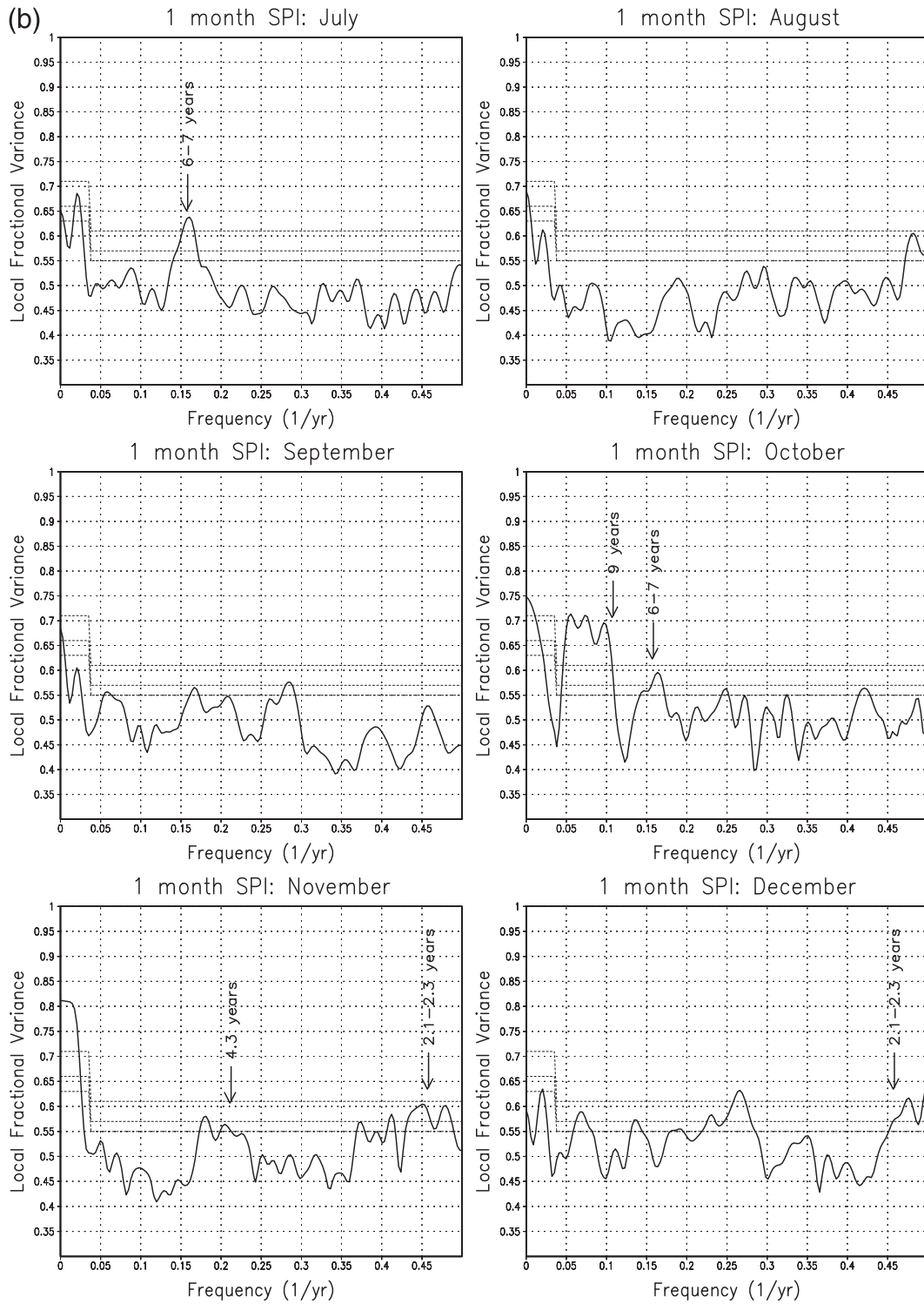
FIG. 4. (*Continued*)

with an increase in the number of retained PCs. CCA analyses are performed as a check to confirm the fact that strong covariability exists between precipitation and land surface variables at specific times of the year.

4. Dominant spatiotemporal patterns of variability and covariability

a. SPI

The LFV spectrum for the complete dataset of the CPC U.S.–Mexico 3-month SPI is shown in Fig. 1. The same analysis of the SPI for time scales from 1 to 6 months was performed, and the results were similar for all cases. The LFV spectrum in Fig. 1 shows significant peaks above the 90% confidence interval at the following approximate time scales: 25, 6–7, 4.3, and 2.1–2.3 yr. In addition, there is a distinct peak at the approximately 9-yr time scale, though it reaches just short of the 90% confidence interval. This peak is important because it relates to soil moisture variability, as will be shown in the next subsection. The reconstructed spatial patterns corresponding to the significant peaks in the LFV spectrum, including the 9-yr peak, are shown in Fig. 2. Notice that the reconstructed spatial pattern corresponding to the 25-yr time scale is omitted in Fig. 2 because it is not distinct from a trend, and drastic differences can be seen in the spatial pattern at the U.S.–Mexico border related to the quality of the Mexican precipitation data, as mentioned in Castro et al. (2007b).

Of greatest interest are the 6–7- and 9-yr bands, because they approximately correspond with the significant variability in vegetation and soil moisture, respectively, as will be shown in the next subsections. The 3-month SPI within the 6–7 band is tied to variability in Pacific sea surface temperatures. The spatial pattern reflects the well-known North American cool-season precipitation relationships associated with ENSO (e.g., Ropelewski and Halpert 1986). In-phase precipitation anomalies with the reference grid point are strongest in the central and southwestern United States (more precipitation is favored in an El Niño year). Out-of-phase anomalies are strongest in the Pacific Northwest and Tennessee and Ohio River Valleys (more precipitation favored in a La Niña year). The 9-yr band, on the other hand, does not bear a resemblance to the traditional ENSO-related precipitation pattern. Rather, precipitation anomalies are generally in phase with the reference grid point everywhere and are maximized in the central United States. This is important because it indicates that anomalously wet or dry conditions associated with this frequency band are generally experienced throughout the entire contiguous United States, and not just con-

fined to one region. The other higher frequency bands at 4.3 and 2.1–2.3 yr also do not bear much resemblance to the ENSO precipitation pattern. Similar higher-frequency signals were not found in soil moisture or vegetation, so these are of much lesser interest.

The LFV spectra for the 3- and 1-month SPI by month are shown in Figs. 3 and 4 , respectively. Notice in these figures that only the statistically significant peaks that appear in the entire dataset in Fig. 1 are highlighted and that the same statistical confidence intervals are used. The analysis of the data in this way for the different SPI time scales reveals several interesting points that cannot be ascertained from an analysis of the entire dataset in Fig. 1. The statistically significant signals in the 3-month SPI are mostly related to cool-season precipitation (fall through spring), as the most statistically significant signals in the monthly LFV spectra appear in this window. There is statistically significant variability in the SPI at the relatively low 9–12-yr frequency during the fall months; the higher-frequency 4.3 and 2.1–2.3-yr signals appear most predominantly in January, February, and March, and the 6–7-yr (ENSO related) signal is apparent in March, April, and May. There is little, if any, statistically significant signal in the 3-month SPI during the warm season, except in September, when there is a weakly significant signal (barely exceeding the 90% confidence interval) in 6–7-yr band.

Considering the monthly LFV spectra for the 1-month SPI (Fig. 4), peaks in the LFV spectra described earlier for the 3-month SPI are generally less significant. Of greatest interest is that the 6–7-yr signal is no longer significant in the spring months, with the exception of May. There are two months, however, when large and very statistically significant signals (exceeding the 99% confidence interval) appear that do not exist in the 3-month SPI. The first occurs during the month of July at a time scale of 6–7 yr. This signal then completely disappears during the month of August. The second occurs during the month of October at a time scale of approximately 9–15 yr. These very strong signals in the 1-month SPI are realized as more muted signals in the 3-month SPI monthly LFV spectra in subsequent months. The 1-month July SPI signal appears in the 3-month September SPI, and the 1-month October SPI signal appears in the 3-month November SPI and the 3-month December SPI. It will be shown that the variability in the SPI for these periods is the key reason for the long-term soil moisture and vegetation variability.

The reconstructed spatial patterns corresponding to these two signals for the 1- and 3-month SPI are fairly consistent and are shown in Fig. 5. The 1-month July SPI and the 3-month September SPI signal correspond to significant variability in summer precipitation at a 6–7-yr
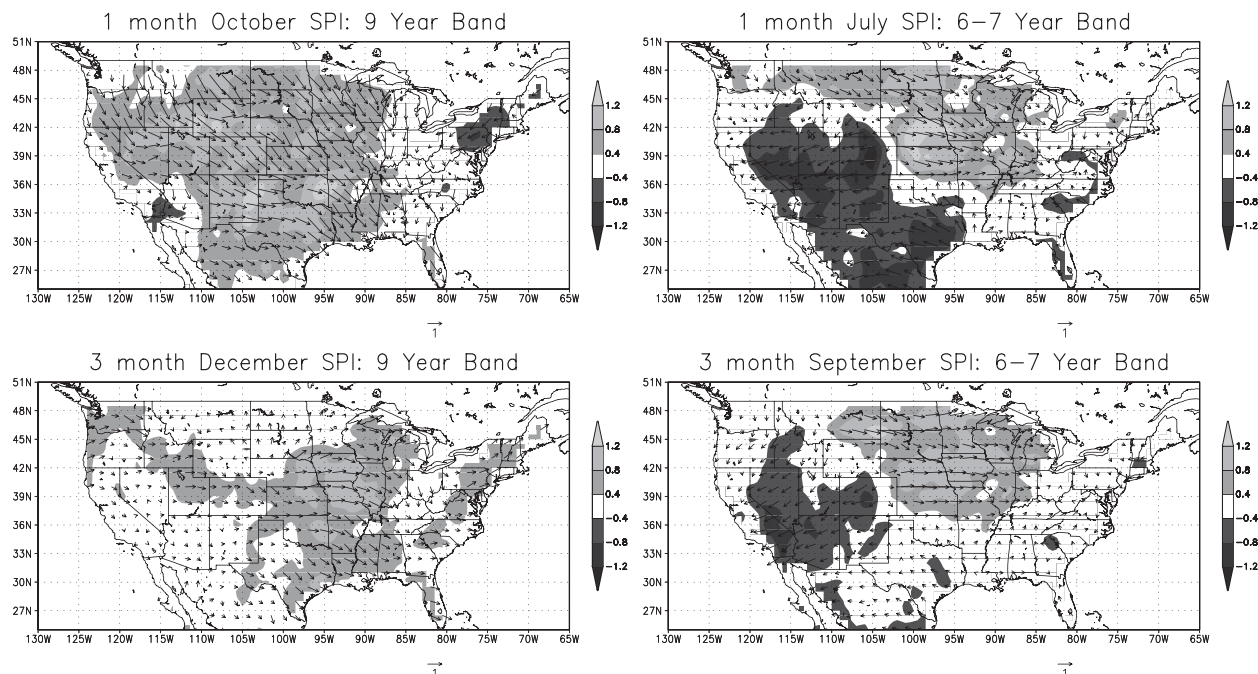
FIG. 5. Same as Fig. 2 but for specific 1- and 3-month SPI signals in monthly data from Figs. 3 and 4 that correspond to significant spatiotemporal variability in soil moisture and vegetation greenness. Vector length is 1.

time scale. Though this is the same time scale that corresponds with the winter ENSO precipitation signal as shown in Fig. 2, the spatial pattern is completely different. Precipitation anomalies in phase with the reference grid point occur throughout the central United States, and out phase anomalies occur throughout the southwestern United States. This spatial pattern of precipitation variability in the warm season is a consequence of time-evolving teleconnections associated with Pacific SSTAs that affect the timing of the NAMS. As shown in Figs. 8 and 9 of Castro et al. (2007b), these teleconnections significantly affect precipitation over the United States during the monsoon onset period in late June and July, but then they quickly wane in August. The dramatic change in the 1-month SPI LFV spectra between July and August shown in Fig. 4 is completely consistent with this idea. The 1-month October SPI and the 3-month December SPI signals correspond to significant variability in fall precipitation at the approximately 9–12-yr time scale. As previously mentioned, this signal does appear as a peak in the complete 3-month SPI LFV spectrum in Fig. 2, though it is not significant at the 90% confidence interval.

b. VIC and Noah soil moisture

The LFV spectrum for normalized VIC soil moisture, considering the entire period of record, is shown in Fig. 6. A significant peak (exceeding the 95% confidence

interval) in the spatiotemporal variability occurs at approximately the 9-yr time scale. Another significant peak occurs at approximately 25 yr, but this peak is discounted because it is not distinguishable from a long-term trend and its corresponding spatial pattern reflects data quality problems at the U.S.–Mexico border. The same analysis was performed on the Noah soil moisture with a similar result (also shown in Fig. 6), though the 9-yr peak is barely significant at the 90% confidence level. However, given the fact that Noah and VIC are different land surface models and the analysis periods considered are slightly different, the comparison is still quite good.

The spatial pattern corresponding to the 9-yr band for VIC soil moisture is shown in Fig. 7. The spatial pattern is very similar to the 9-yr band in the 3-month SPI previously shown in Fig. 2, with variability again maximized in the central United States. A similar result was obtained with the Noah soil moisture data (not shown). In the central United States, soil moisture can vary approximately 10%–20% around its climatological value with respect to variability at this time scale. Consideration of the VIC soil moisture LFV spectrum by month (Fig. 8) shows that the significant 9-yr signal occurs only in November and December, just as in the 3-month SPI (cf. Fig. 3). CCA was performed on the average of the 3-month November and December SPI and the average of November and December VIC soil moisture.
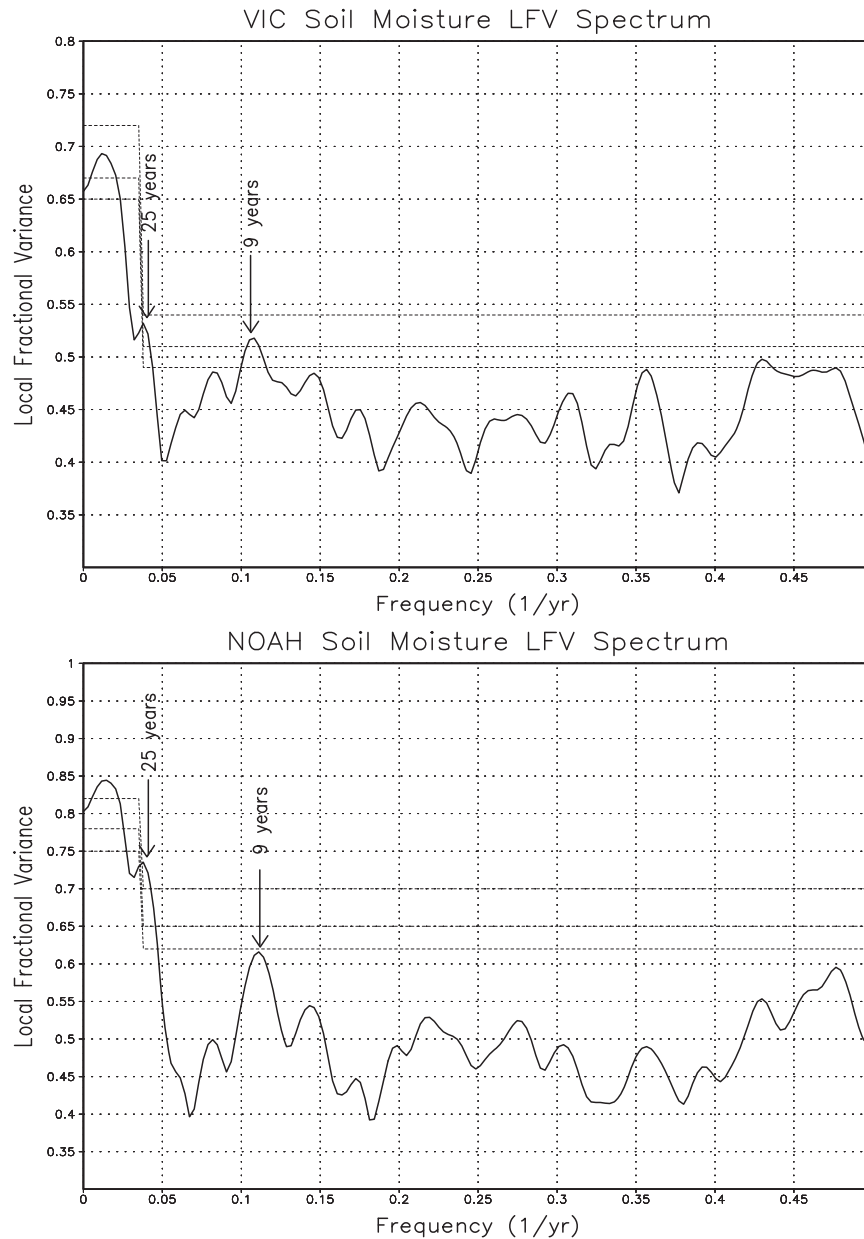
FIG. 6. Same as Fig. 1 but for VIC soil moisture (1950–2000) and Noah soil moisture (1948–98).

Fourteen principal components were retained to generate a canonical correlation of 0.48 for the first mode. The homogeneous correlation maps for the first canonical vector are shown in Fig. 9. The first canonical correlation indicates a continental-scale pattern of rainfall positively related with soil moisture, and the covariability with soil moisture is strongest in the central United States. This result is generally consistent with the spatial patterns of the SPI (Fig. 2) and soil moisture (not shown) variability at the 9-yr time scale in the fall season from MTM–SVD. Therefore, significant long-term

spatiotemporal variability in soil moisture in the contiguous United States appears to be related to decadal variability in late fall to early winter precipitation.

The time series of VIC soil moisture and the 3-month SPI in the 9-yr band with respect to the reference grid point (Fig. 10) show minima in the mid-1950s, mid-1960s, late 1970s, late 1980s to early 1990s, and late 1990s to early 2000s. In general, these periods correspond very well to the aforementioned periods of drought in the central and western United States mentioned in the introduction, with the longest of these
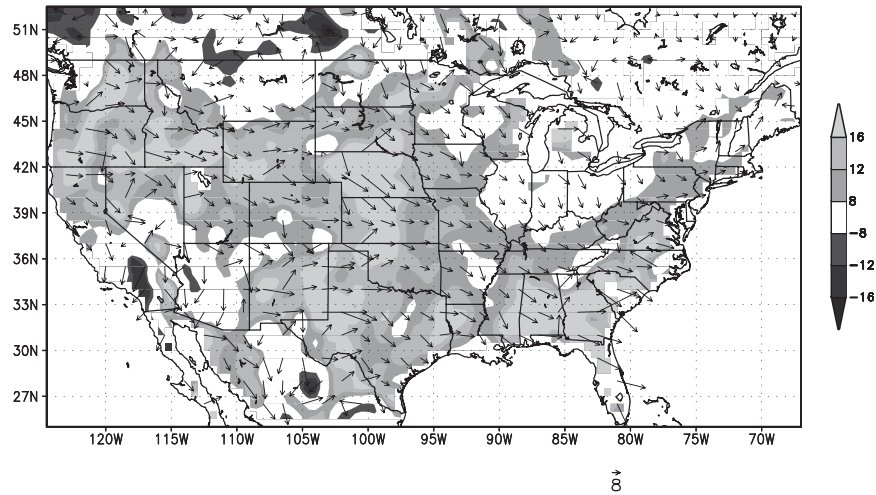
FIG. 7. Same as Fig. 2 but for VIC soil moisture. Vector magnitude and in-phase projection shading expressed as a percentage difference from the soil moisture climatology. Vector length is 8%.

droughts being in the mid-1950s and late 1990s to early 2000s. As evidenced by the aforementioned references with respect to both global model simulations and the paleoclimate record, the occurrence of such droughts is driven by La Niña–like conditions in the tropical Pacific and/or warm SSTs in the Indian Ocean. As Fig. 7 suggests, the drought signal during such times is generally coherent throughout the contiguous United States and maximized in the central and western United States. This is certainly true of the most severe droughts in the paleoclimate (i.e., tree ring) record (Herweijer et al. 2007).

c. GIMMS NDVI

The LFV spectrum for the entire record of normalized U.S.–Mexico NDVI is shown in Fig. 11. Notice that because the NDVI record is about half the length of the soil moisture record, only spatiotemporal variability on a time scale less than about 10 yr can be assessed. Even given the relatively short length of the NDVI record, a fairly significant peak in the LFV spectrum is present at the 6–7-yr time scale (exceeding the 95% confidence interval). Recall that this is the time scale that is associated with both the well-known ENSO precipitation signal in late spring and the distinctly different early summer precipitation signal associated with the NAMS, also related to Pacific SSTAs. If, similar to soil moisture, the spatiotemporal variability of vegetation greenness is tied to the precipitation variability at the same time scale, the question is then which of the two precipitation signals in the 6–7-yr band is more strongly related to vegetation: the one in spring or the one in early summer?

The spatial pattern corresponding to the 6–7-yr band for the entire NDVI record is shown in Fig. 12. Although the percentage differences in NDVI from climatology are modest compared to soil moisture, it is the spatial pattern of variability that is probably more important. The largest signals in NDVI variability (greater than 10% difference from climatology) occur in the southern Great Plains, north-central Mexico, and the southwestern United States. There is a strong out-of-phase relationship between these regions, and the contrast between them is quite sharp in terms of their relative distance from each other. We note that the spatial pattern is not entirely consistent over areas where irrigation may be a large contributing factor in vegetation greenness (Ozdogan and Gutman 2008). Namely, in the Great Plains, the signal abruptly changes for a few locally isolated grid points. Despite this, the spatial pattern as a whole still appears to reflect differences in precipitation associated with the NAMS with respect to Pacific SSTAs—and not the late spring signal. The month-by-month LFV spectra of NDVI confirm this conclusion (Fig. 13). There is no statistically significant signal in the 6–7-yr band until the month of August, and the spatial pattern of August NDVI in the 6–7-yr band is nearly identical to Fig. 12 (not shown). It should also be noted that a statistically significant signal in NDVI occurs in October, but its spatial pattern does not resemble Fig. 11 (not shown). It is the NDVI during the warm season that is more important, in any case, as this is the period of where vegetation greenness is at a maximum. Though the statistically significant signal in summer precipitation variability occurs in July and then disappears, according to the 1-month SPI (Fig. 4), the response in
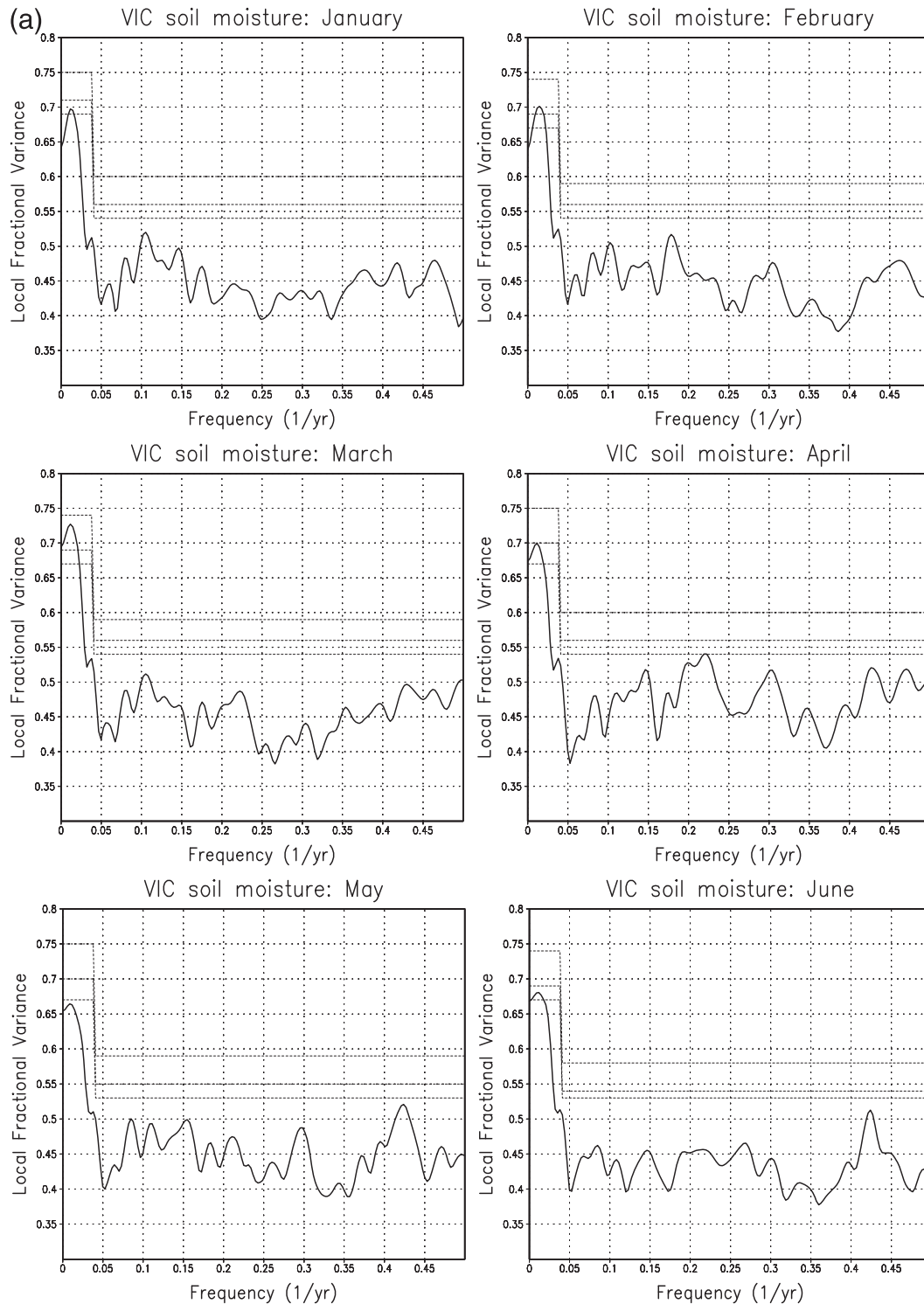
FIG. 8. Same as Fig. 3 but for VIC soil moisture.

the vegetation occurs one month later in August. Thus, the vegetation greenness appears to respond to variability in precipitation with a delay of several weeks to a month. As mentioned, the vegetation response to pre- cipitation in individual years in the core NAMS region also has a similar time delay (Watts et al. 2007), thus the results here are quite physically reasonable, especially given the biweekly time resolution of the NDVI
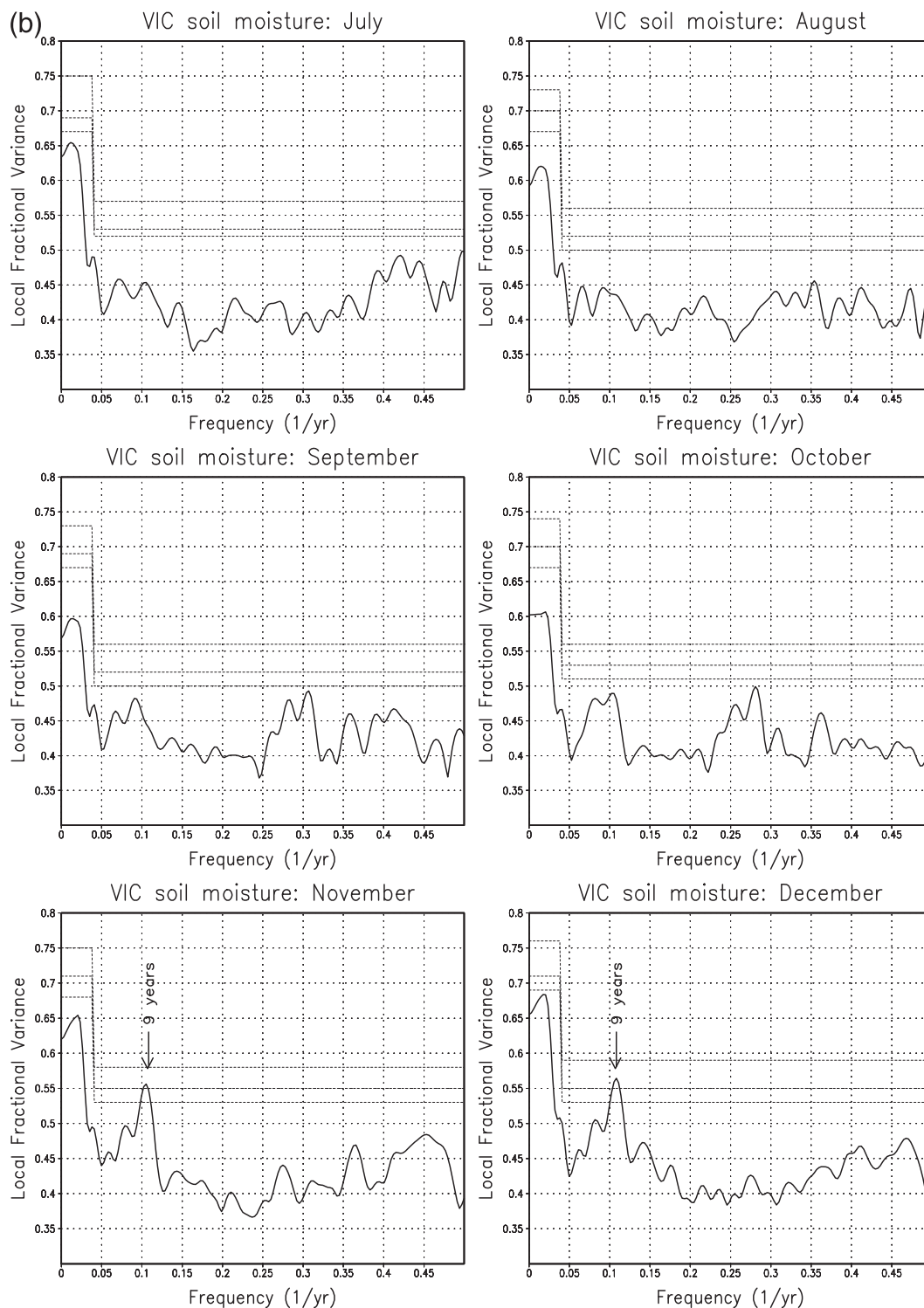
(b)

FIG. 8. (*Continued*)

product. To confirm this linkage between early summer precipitation and NDVI, CCA was performed on the 1-month July SPI and August NDVI. Retaining the first eight principal components, the canonical correlation of the first mode is 0.47, and the homogeneous correlation maps are shown in Fig. 14. The first canonical correlation clearly reflects an inverse relationship for both precipitation and vegetation greenness between the
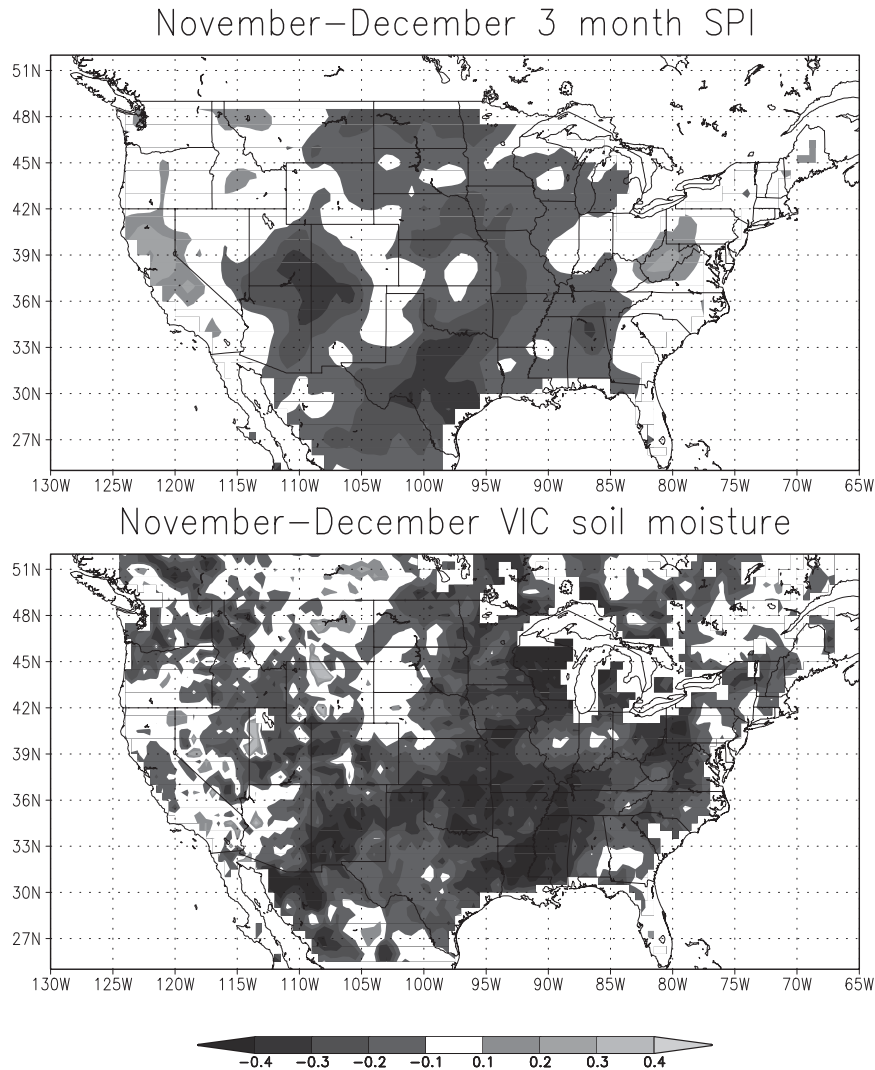
FIG. 9. Homogeneous correlation maps of average November–December (top) 3-month SPI and (bottom) VIC soil moisture with first canonical correlation vector. Fourteen PCs are retained in the CCA. The canonical correlation of this first mode is 0.48.

central United States and the core monsoon region that is consistent with remote Pacific SST forcing (e.g., Castro et al. 2001, 2007b), even given the relative short satellite observational record. The relationship of August vegetation greenness to early summer precipitation is also consistent with a 2100-yr tree-ring record from El Malpais, New Mexico, which constructed cool- and warm-season precipitation considering early versus late wood tree-ring growth (Stahle et al. 2009). This paleoclimate record shows distinctly different interannual variability in the summer monsoon precipitation signal there compared to the cool season and a connection of monsoon precipitation to Pacific SSTAs in a manner consistent with the aforementioned modern record. Though it is just from one location, the El Malpais record strongly

suggests that the vegetation response in Figs. 12 and 14 is a robust feature of NAMS interannual variability that has existed for thousands of years.

Aside of the likely influence of irrigation, there is one more subtle, but important, characteristic to the NDVI spatial pattern maps in Figs. 11 and 14. The stronger vegetation response to interannual variability of monsoon precipitation generally occurs at lower elevations in the western United States. In Arizona, for example, there is very little change in August NDVI from climatology (3% or less) along the Mogollon Rim, the mountain range that extends from approximately the southeast to northwest part of the state (Fig. 12). However, in the low deserts, in the southwest part of the state, the change in NDVI is greater than 10% from
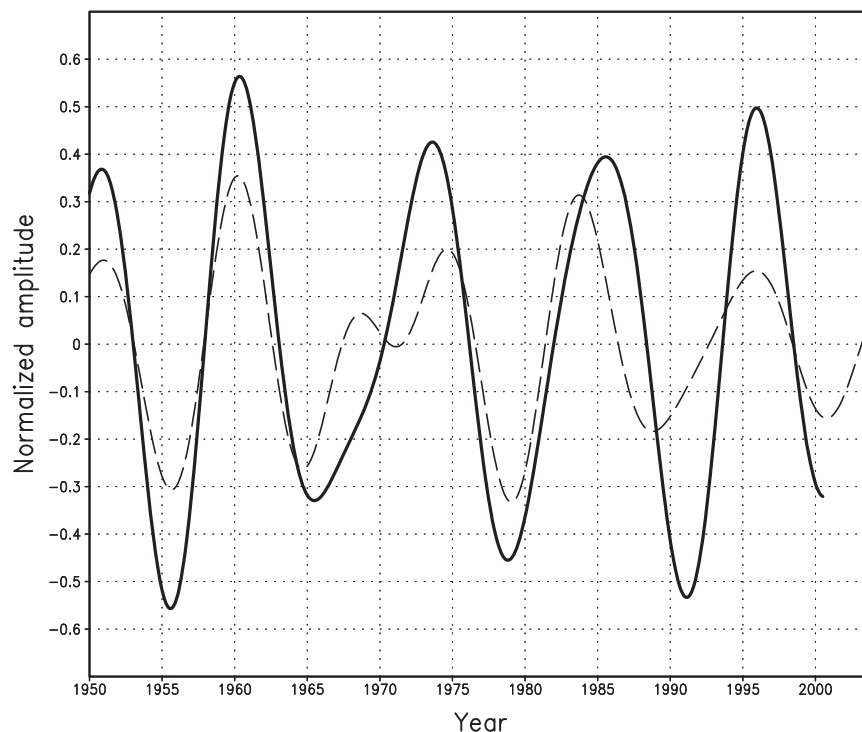
FIG. 10. Time series of reconstructed VIC soil moisture (solid) and 3-month SPI (dashed) in the 9-yr band at the central U.S. reference grid point (36°N, 97.5°W). Period is 1950–2003.

climatology (Fig. 12). Though it is a desert, there is still quite a bit of vegetation cover and, as mentioned, this area can green up relatively quickly after substantial monsoon rains. Recent research by Bieda et al. (2009) also shows that wetter monsoon years are characterized by an increased occurrence of synoptic disturbances in the southwestern United States. This is a typically necessary condition to cause terrain-induced convection to organize and propagate westward toward the Colorado River Valley and Gulf of California.

5. Conclusions and discussion

The main goal of the present study is to determine the dominant spatiotemporal patterns of precipitation that force long-term variability in soil moisture and vegetation. The analysis procedure used three statistical techniques. First, all the variables analyzed were normalized according to the SPI procedure. The SPI transformation works well for precipitation, and, by extension, land surface variables forced by precipitation because they do not exhibit normal distributions. This is especially true in the drier climates of the western United States. Second, the dominant patterns of spatiotemporal variability in all variables were determined using MTM–SVD for interannual and longer time scales. Separate

MTM–SVD analyses considered the entire length of a given data record and individual months. Third, the CCA technique is used to assess the covariability between the SPI, soil moisture, and vegetation greenness.

The MTM–SVD analyses of the SPI at 1- and 3-month time scales produce physically reasonable spatiotemporal patterns that generally conform to Pacific SST forcing on interannual and longer time scales. Two specific time scales were emphasized that correspond to significant spatiotemporal variability in soil moisture and vegetation. First, there is a 9-yr signal that is associated with maximum precipitation anomalies in the central United States and in-phase precipitation anomalies over most of the rest of the country. This signal is related to variability in precipitation in the late fall to early winter period and is associated with the occurrence of major droughts in North America, such as in the mid-1950s and late 1990s to early 2000s. The significant spatiotemporal variability in soil moisture corresponds to this precipitation forcing, and the signal is present in both the VIC and Noah data. Second, there is a 6–7-yr signal that is associated with two distinctly different patterns of precipitation anomalies in the cool and warm seasons. The cool-season pattern is more reflective of wintertime precipitation relationships with ENSO. This is the dominant pattern when considering the entire
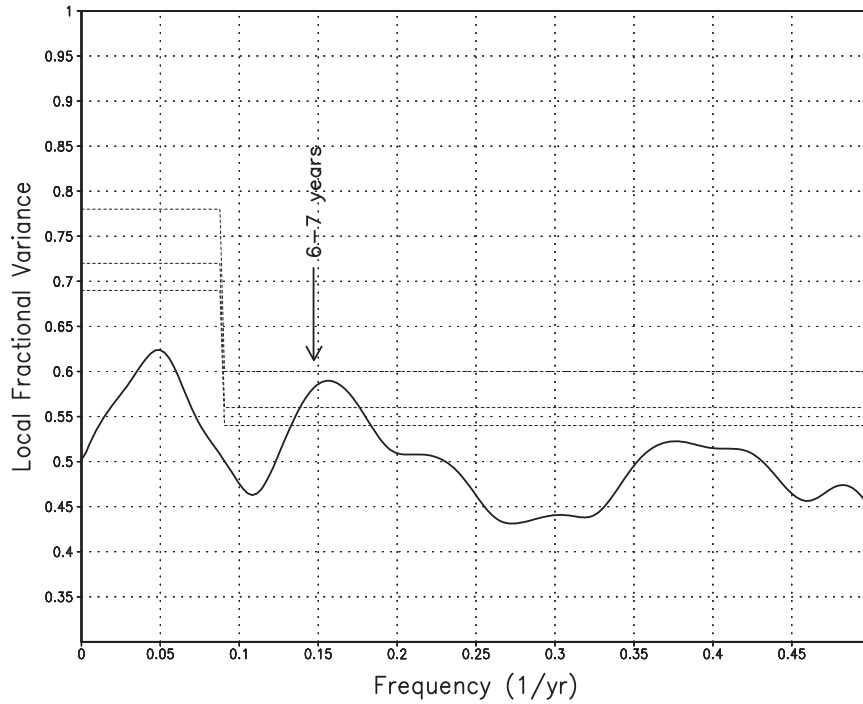
Fig. 11. Same as Fig. 1 but for GIMMS NDVI (1982–2003).

precipitation record. The warm season pattern is reflective of the interannual variability of the NAMS in relation to tropical and north Pacific SSTs, and it is only revealed by analysis of precipitation data by individual month. It is the warm-season monsoon pattern that drives the significant spatiotemporal variability in vegetation, with an approximately 1-month time delay in the vegetation response. A stronger vegetation response occurs at lower elevations in the western United States.

Though these results clearly show that large-scale patterns of land surface variability in North America are forced by the atmosphere on interannual and longer time scales, we emphasize that the potential land surface forcing to the atmosphere has not been explicitly addressed within the present study. Observations and modeling studies have shown that the atmosphere is affected by soil moisture conditions via the exchange of energy and water (e.g., Pielke 2001; Pitman 2003). The effect of antecedent soil moisture
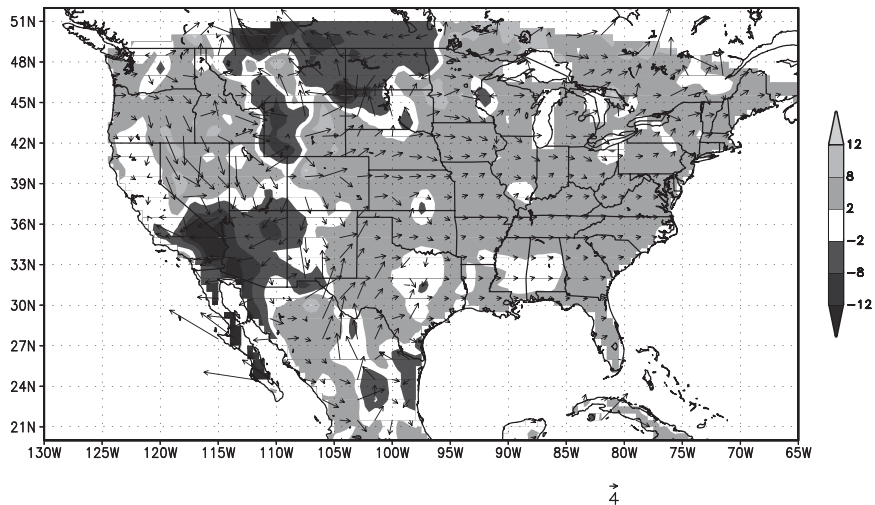

Fig. 12. Same as Fig. 7 but for GIMMS NDVI. Vector length is 4%.

conditions on precipitation could be very important, particularly in the warm season when most of the precipitation is due to convective processes, driven in great part by land surface heterogeneity. The complex nature of the soil moisture–precipitation relationship is quite apparent from recent work that has investigated soil moisture–precipitation feedbacks in North America and globally. Findell and Eltahir (1997) found a positive feedback during the summer using soil moisture observations from Illinois. Other regional climate model (RCM) sensitivity-type studies have also been focused on the central United States, mostly on years with extreme climate conditions, such as the 1988 drought and 1993 flood (e.g., Pan et al. 1996; Hong and Pan 2000). These studies have suggested a positive feedback, but the effect of soil moisture anomalies on precipitation is locally confined. RCM studies have investigated the core monsoon region with similar results (e.g., Small 2001; Kanamitsu and Mo 2003). However, other work suggests that there may be no feedback, (e.g., Georgakakos et al. 1995; Salvucci et al. 2002) or that the feedback may actually be negative (e.g., Giorgi et al. 1996; Paegle et al. 1996; Wei et al. 2008). Of relevance to the conclusions here, Wei et al. (2008) recently showed that within the context of a general circulation model, intraseasonal variability in precipitation has a negative relationship with antecedent soil moisture. They attribute this to the fact that intraseasonal variability is dominated by global-scale atmospheric oscillations that are entirely independent of land surface forcing.

Limitations inherent to observational and modeling studies when analyzing soil moisture–precipitation feedbacks include sparse spatial and temporal resolution in soil moisture observations, or lack thereof; model domain size and grid spacing; and model parameterization schemes, such the convective parameterization or boundary layer schemes. In addition, some of the methodologies used have limitations in detecting a feedback signal—namely, the persistence of precipitation cannot be distinguished when using simple lagged correlation analyses. More complex methods of assessing the presence of the signal, such as to test for Granger causality (Salvucci et al. 2002) or nonparametric tests (Alfieri et al. 2008), have recently been used to address the issues of autocorrelation in the precipitation data.

A hypothesis posed in Castro et al. (2001; 2007b) stated that the influence of the land surface forcing, like the remote SST forcing, is time dependent, becoming more important at certain times of the year than others. The late summer period, when the early summer teleconnection Pacific SST–related patterns diminish, is a

good example. At this time, the amount of precipitation due to recycled moisture from land surface soil evaporation and transpiration from plants increases in the core monsoon region and central United States, as suggested by some observational and global modeling studies (e.g., Brubaker et al. 2001; Bosilovich et al. 2003; Dominguez et al. 2008). In particular, Dominguez et al. (2008) applied a dynamical precipitation recycling model to the North American Regional Reanalysis to diagnose the percentage of precipitation due to local surface water vapor fluxes in the core monsoon region through the warm season. The recycled moisture from the land surface becomes more important during the latter part of the summer and can account for up to 20% of the rainfall in mid-August during active monsoon years. Other studies incorporating satellite-derived or dynamic vegetation in RCMs have demonstrated the importance of vegetation, and, like the aforementioned soil moisture RCM studies, these also tend to be sensitivity-type studies focus on one or several years (e.g., Lu and Shuttleworth 2002). In agreement with the hypothesis of a time-varying influence of the land surface forcing, Lu and Shuttleworth (2002) found that with a more realistic model representation of vegetation, increases in precipitation are maximized in the latter part of the summer.

MTM–SVD does work to obtain the significant spatiotemporal patterns on the large continental-scale domain used here. However, if, as RCM studies suggest, the influence of land feedback to the atmosphere is more locally confined, MTM–SVD as used here will not capture this effect. For example, increased vegetation in the core NAMS region during wet monsoon years may supply additional atmospheric moisture during the month of August, as suggested by Lu and Shuttleworth (2002) and Dominguez et al. (2008). Rainfall, therefore, may increase locally because of this additional moisture, through the creation of local thunderstorms and mesoscale convective systems (e.g., Carleton et al. 2008a,b), but the effect will be generally confined to the area where the enhanced vegetation growth occurs and may not contribute to any statistically significant pattern on a continental scale. Our future work will incorporate the satellite-derived NDVI product used here in the warm-season regional climate model simulations of Castro et al. (2007b), replacing the climatological specification of vegetation used in those original model simulations. Analysis of precipitation from these new model simulations should reveal whether a more realistic representation of vegetation has an effect on model-simulated rainfall patterns and amount for the period of the satellite NDVI record, particularly in the latter part of the summer.
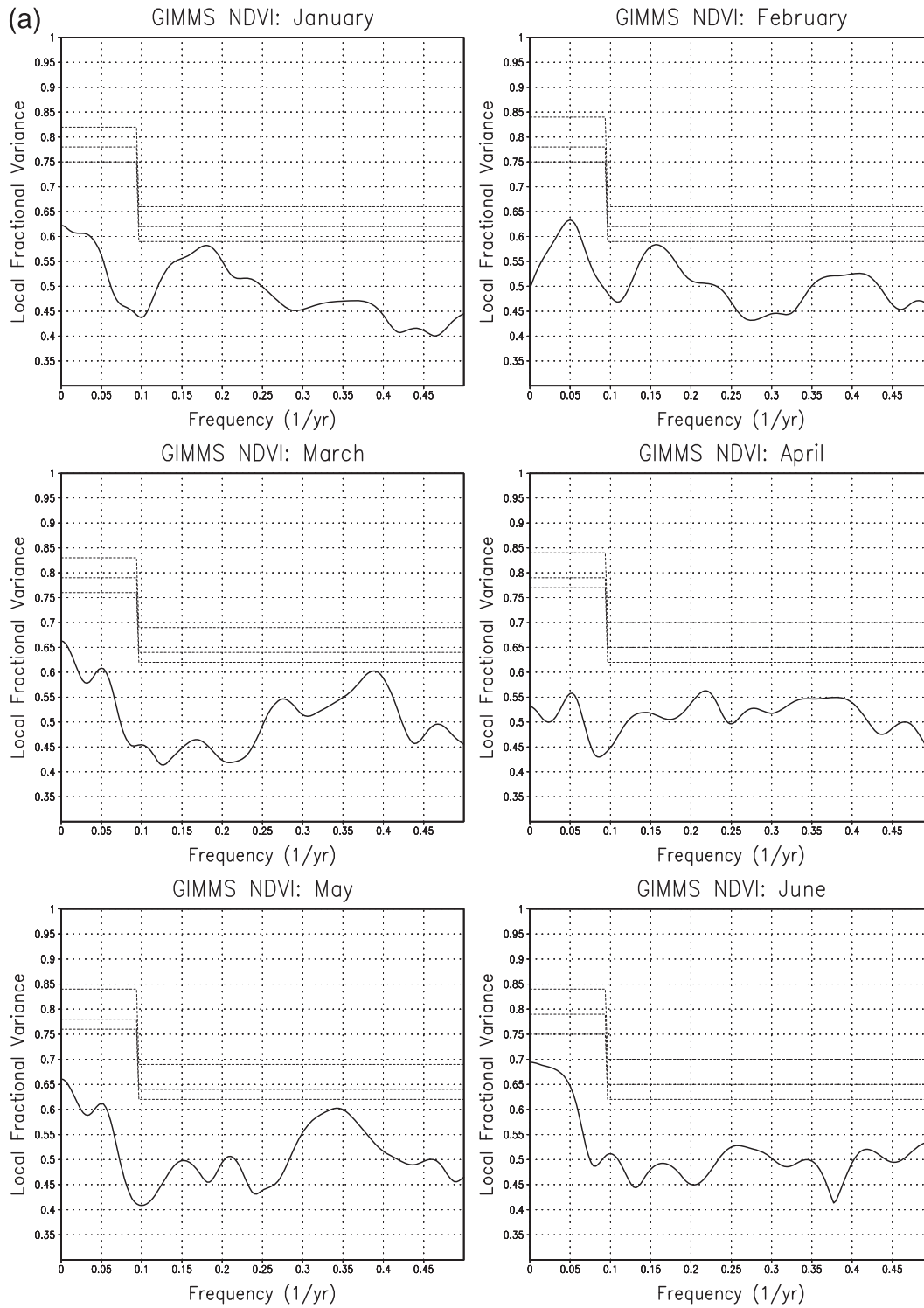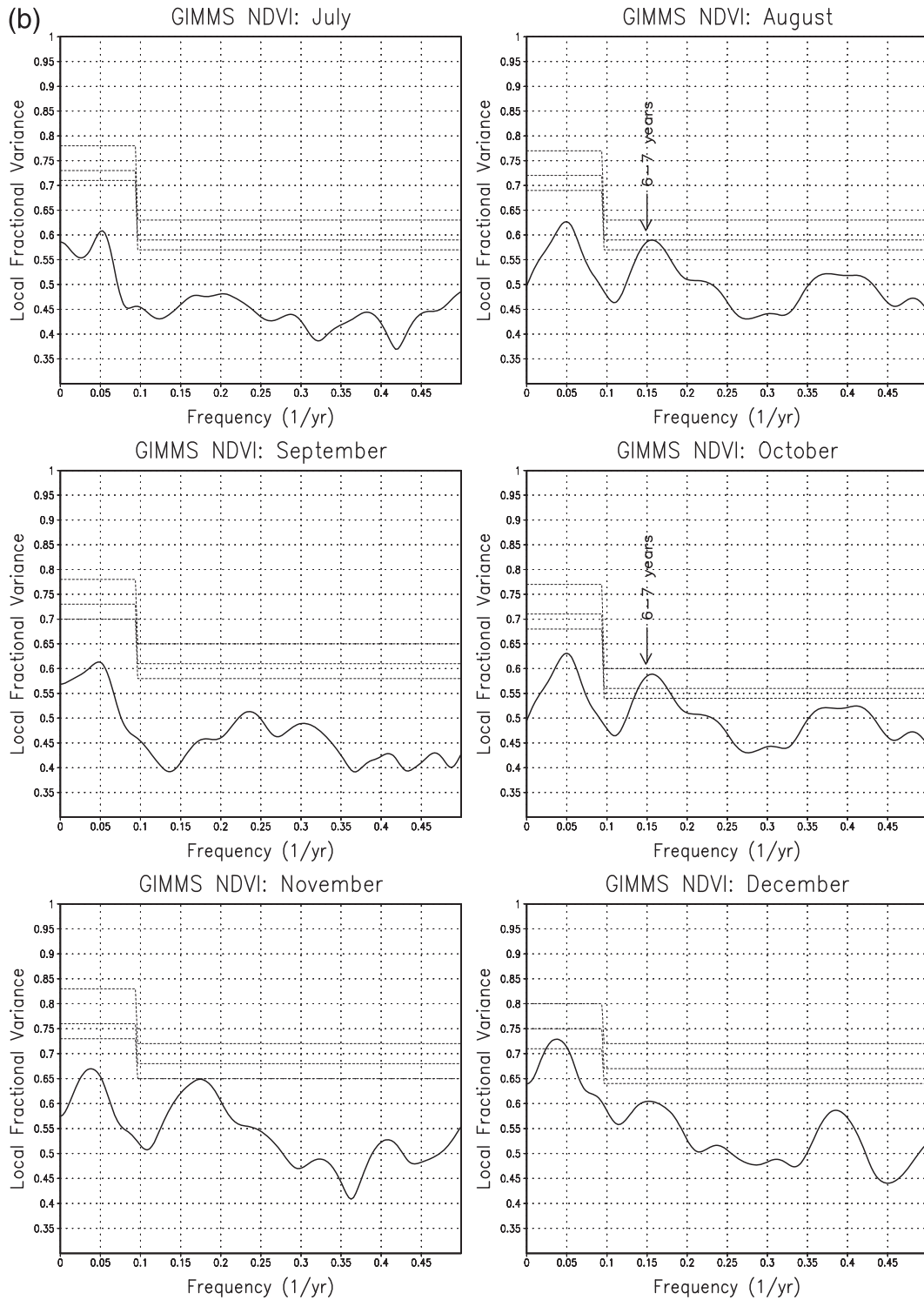
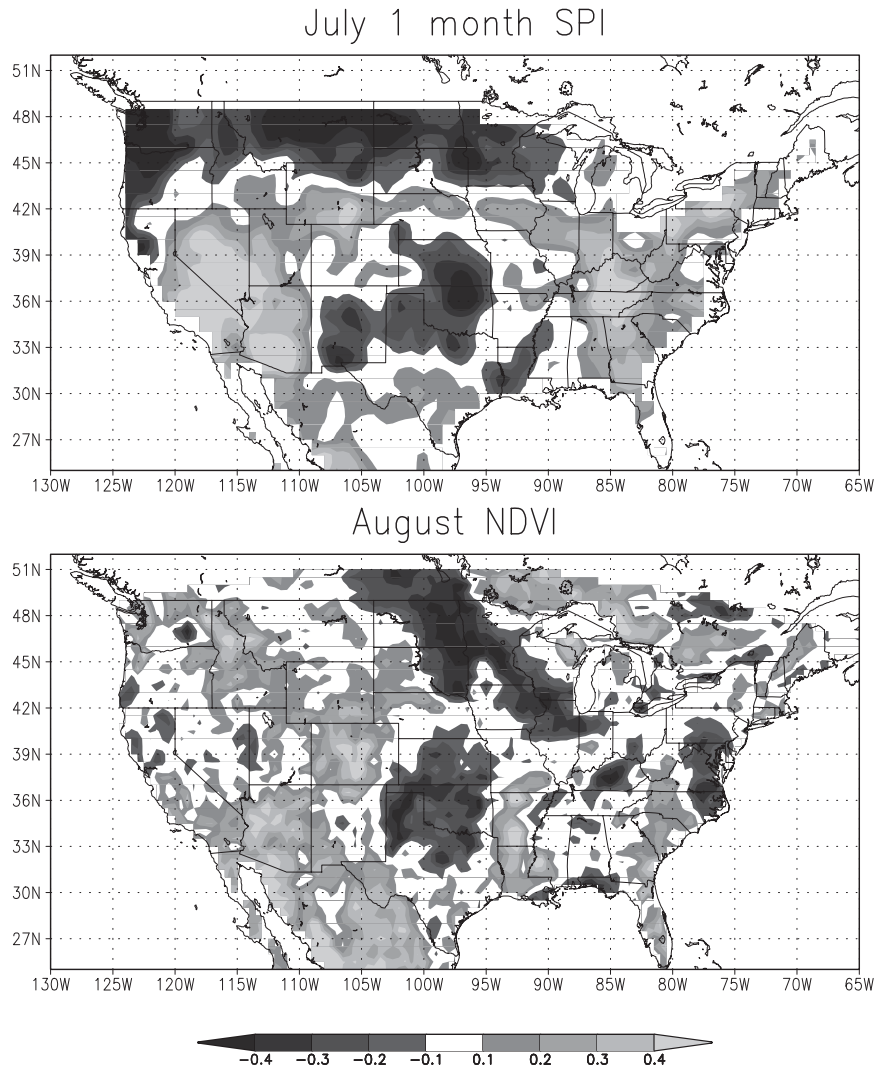FIG. 13. Same as Fig. 3 but for GIMMS NDVI.

FIG. 13. (*Continued*)

FIG. 14. Homogeneous correlation maps of the (top) 1-month July SPI and (bottom) August NDVI with first canonical correlation vector. Eight PCs are retained in the CCA. The canonical correlation of this first mode is 0.47.

APPENDIX

Summary of the MTM–SVD Method

The following is a brief summary of the MTM–SVD method and follows from Mann and Park (1994, 1996) and Rajagopalan et al. (1998). The specific analysis routines are freely available online from Dr. Michael Mann at the Pennsylvania State University and are the same used in Rajagopalan et al. (1998). An identical summary was also given in Castro et al. (2007b).

For the given time series y (SPI, soil moisture, or NDVI, in this case) a set of K orthogonal data tapers and K-associated tapered Fourier transforms (eigenspectra) is determined at each frequency f by

$$Y_k^{(m)}(f) = \sum_{t=1}^{N} w_t^{(k)} y_n e^{i2\pi ft\Delta t}, \qquad \text{(A1)}$$

where Δt is the sampling interval (1 month); $\left\{ w_t^{(k)} \right\}_{t=1}^{N}$ is the kth member in an orthogonal series of (Slepian) data tapers, $k = 1, \ldots, K$; $m = 1, \ldots, M$ are the number of grid points with data; and N is the length of the time series. Only the first $k = 2p - 1$ data tapers are usefully resistant to spectral leakage. A choice of $p = 2$ and $k = 3$ tapers is used, as it provides good frequency resolution and sufficient spectral degrees of freedom. At each frequency point, the $M \times K$ matrix is

$$\mathbf{A}(f) = \begin{bmatrix} w_1 Y_1^{(1)} & w_1 Y_2^{(1)} & \ldots & w_1 Y_K^{(1)} \\ w_2 Y_1^{(2)} & w_2 Y_2^{(2)} & \ldots & w_2 Y_K^{(2)} \\ \ldots & \ldots & \ldots & \ldots \\ w_M Y_1^{(M)} & w_M Y_2^{(M)} & \ldots & w_M Y_K^{(M)} \end{bmatrix}, \qquad \text{(A2)}$$

where w represent gridpoint-specific weightings for latitude. A complex SVD is performed on the previous matrix,

$$\mathbf{A}(f) = \sum_{k=1}^{K} \lambda_k(f)\mathbf{u}_k(f) \otimes \mathbf{v}_k^*(f), \qquad \text{(A3)}$$

where an asterisk denotes the complex conjugate. Here, λ_k describes the relative fraction of total variance explained by the kth mode, its associated left eigenvector $\mathbf{u}_k^*$ represents the spatial EOFs, and $\mathbf{v}_k$ describes the spectral EOFs.

Within the scale of resolvable frequencies, the fractional variance explained by the kth mode, or LFV, is $\lambda_k^2 / \sum_{j=k}^{K} \lambda_j^2$. Significance of peaks in the LFV spectrum are obtained through a bootstrapping procedure in which the noise at each gridpoint time series is assumed locally white over the bandwidth of eigentapers. In the bootstrap procedure, the spatial fields are randomly resampled 1000 times. The reconstruction of the spatiotemporal signal corresponding to the statistically significant frequencies in the LFV spectrum is described in appendix B of Mann and Park (1994).

REFERENCES

Alfieri, L., P. Claps, P. D'Odorico, F. Laio, and T. M. Over, 2008: An analysis of the soil moisture feedback on convective and stratiform precipitation. *J. Hydrometeor.,* **9,** 280–291.

Andreadis, K. M., and D. P. Lettenmaier, 2006: Trends in 20th century drought over the continental United States. *Geophys. Res. Lett.,* **33,** L10403, doi:10.1029/2006GL025711.

——, E. A. Clark, A. W. Wood, A. F. Hamlet, and D. P. Lettenmaier, 2005: Twentieth-century drought in the conterminous United States. *J. Hydrometeor.,* **6,** 985–1001.

Barnett, T. P., and R. W. Preisendorfer, 1987: Origins and levels of monthly seasonal forecast skill for United States surface air temperatures determined by canonical correlation analysis. *Mon. Wea. Rev.,* **115,** 1825–1850.

Bieda, S. W., III, C. L. Castro, S. L. Mullen, A. Comrie, and E. Pytlak, 2009: The relationship of transient upper-level troughs to variability of the North American monsoon system. *J. Climate,* **22,** 4213–4227.

Bosilovich, M. G., Y. C. Sud, S. D. Schubert, and G. K. Walker, 2003: Numerical simulation of the large-scale North American monsoon water sources. *J. Geophys. Res.,* **108,** 8614, doi:10.1029/2002JD003095.

Brubaker, K. L., P. A. Dirmeyer, A. Sudradiat, B. S. Levy, and F. Bernal, 2001: A 36-yr climatological description of the evaporative sources of warm-season precipitation in the Mississippi River basin. *J. Hydrometeor.,* **2,** 537–557.

Carleton, A. M., D. L. Arnold, D. J. Travis, S. Curran, and J. O. Adegoke, 2008a: Synoptic circulation and land surface influences on convection in the Midwest U.S. "Corn Belt" during the summers of 1999 and 2000. Part I: Composite synoptic environments. *J. Climate,* **21,** 3389–3415.

——, D. J. Travis, J. O. Adegoke, D. L. Arnold, and S. Curran, 2008b: Synoptic circulation and land surface influences on convection in the Midwest U.S. "Corn Belt" during the summers of 1999 and 2000. Part II: Role of vegetation boundaries. *J. Climate,* **21,** 3617–3641.

Castro, C. L., T. B. McKee, and R. A. Pielke Sr., 2001: The relationship of the North American monsoon to tropical and North Pacific sea surface temperatures as revealed by observational analyses. *J. Climate,* **14,** 4449–4473.

——, R. A. Pielke Sr., and J. O. Adegoke, 2007a: Investigation of the summer climate of the contiguous United States and Mexico using the Regional Atmospheric Modeling System (RAMS). Part I: Model climatology (1950–2002). *J. Climate,* **20,** 3844–3865.

——, ——, ——, S. D. Schubert, and P. J. Pegion, 2007b: Investigation of the summer climate of the contiguous United States and Mexico using the Regional Atmospheric Modeling System (RAMS). Part II: Model climate variability. *J. Climate,* **20,** 3866–3887.

Chase, T. N., R. A. Pielke Sr., T. G. F. Kittel, R. Nemani, and S. W. Running, 1996: The sensitivity of a general circulation model to global changes in leaf area index. *J. Geophys. Res.,* **101,** 7393–7408.

Dominguez, F., P. Kumar, and E. R. Vivoni, 2008: Precipitation recycling variability and ecoclimatological stability—A study using NARR data. Part II: North American monsoon region. *J. Climate,* **21,** 5187–5203.

Edwards, D. C., and T. B. McKee, 1997: Characteristics of 20th century drought in the United States at multiple timescales. Department of Atmospheric Science, Colorado State University, Climatology Rep. 97-2, Paper 634, 155 pp.

Fan, Y., H. M. Van den Dool, D. Lohmann, and K. Mitchell, 2006: 1948–98 U.S. hydrological reanalysis by the Noah Land Data Assimilation System. *J. Climate,* **19,** 1214–1237.

Findell, K., and E. A. B. Eltahir, 1997: An analysis of the soil moisture-rainfall feedback, based on direct observations from Illinois. *Water Resour. Res.,* **33,** 725–735.

Georgakakos, K., D.-H. Bae, and D. R. Cayan, 1995: Hydroclimatology of continental watersheds 1. Temporal analyses. *Water Resour. Res.,* **31,** 655–675.

Giorgi, F., L. O. Mearns, C. Shields, and L. Mayer, 1996: A regional model study of the importance of local versus remote controls

of the 1988 drought and the 1993 flood over the central United States. *J. Climate,* **9,** 1150–1162.

Grantz, K., B. Rajagopalan, M. Clark, and E. Zogona, 2007: Seasonal shifts in the North American monsoon. *J. Climate,* **20,** 1923–1935.

Heim, R. R., 2002: A review of twentieth-century drought indices used in the United States. *Bull. Amer. Meteor. Soc.,* **83,** 1149–1165.

Herweijer, C., R. Seager, E. R. Cook, and J. Emile-Geay, 2007: North American droughts of the last millennium from a gridded network of tree-ring data. *J. Climate,* **20,** 1353–1376.

Higgins, R. W., J. E. Janowiak, and Y.-P. Yao, 1996: A gridded hourly precipitation data base for the United States (1963-1993). *NCEP/Climate Prediction Center Atlas 1,* 47 pp.

Hong, S. Y., and H. L. Pan, 2000: Impact of soil moisture anomalies on seasonal summertime circulation over North America in a regional climate model. *J. Geophys. Res.,* **105** (D24), 29 625–29 634.

Hu, Q., and S. Feng, 2002: Interannual rainfall variations in the North American summer monsoon region: 1900–98. *J. Climate,* **15,** 1189–1202.

Huang, N. E., and S. S. P. Shen, Eds., 2005: *Hilbert–Huang Transform and Its Applications.* Vol. 5. World Scientific, 311 pp.

Kanamitsu, M., and K. C. Mo, 2003: Dynamical effect of land surface processes on summer precipitation over the southwestern United States. *J. Climate,* **16,** 496–503.

Lotsch, A., M. A. Friedl, B. T. Anderson, and C. J. Tucker, 2003: Coupled vegetation-precipitation variability observed from satellite and climate records. *Geophys. Res. Lett.,* **30,** 1774, doi:10.1029/2003GL017506.

——, ——, ——, and ——, 2005: Response of terrestrial ecosystems to recent Northern Hemispheric drought. *Geophys. Res. Lett.,* **32,** L06705, doi:10.1029/2004GL022043.

Lu, L., and W. J. Shuttleworth, 2002: Incorporating NDVI-derived LAI into the climate version of RAMS and its impact on regional climate. *J. Hydrometeor.,* **3,** 347–362.

Mann, M. E., and J. Park, 1994: Global scale modes of surface temperature variability on interannual to century time scales. *J. Geophys. Res.,* **99,** 25 819–25 833.

——, and ——, 1996: Joint spatiotemporal modes of surface temperature and sea level pressure variability in the Northern Hemisphere during the last century. *J. Climate,* **9,** 2137–2162.

Maurer, E. P., A. W. Wood, J. C. Adam, D. P. Lettenmaier, and B. Nijssen, 2002: A long-term hydrologically based dataset of land surface fluxes and states for the conterminous United States. *J. Climate,* **15,** 3227–3251.

McKee, T. B., N. J. Doesken, and J. Kleist, 1993: The relationship of drought frequency and duration to time scales. Preprints, *Eighth Conf. on Applied Climatology,* Anaheim, CA, Amer. Meteor. Soc., 179–184.

Mo, K. C., and J. N. Paegle, 2000: Influence of sea surface temperature anomalies on precipitation regimes over the southwest United States. *J. Climate,* **13,** 3588–3598.

Ozdogan, M., and G. Gutman, 2008: A new methodology to map irrigated areas using multi-temporal MODIS and ancillary data: An application example in the continental US. *Remote Sens. Environ.,* **112,** 3520–3537.

Paegle, J., K. C. Mo, and J. Nogués-Paegle, 1996: Dependence of simulated precipitation on surface evaporation during the 1993 United States summer floods. *Mon. Wea. Rev.,* **124,** 345–361.

Pan, Z., E. Takle, M. Segal, and R. Turner, 1996: Influences of model parameterization schemes on the response of rainfall to soil moisture in the central United States. *Mon. Wea. Rev.,* **124,** 1786–1802.

Pitman, A. J., 2003: The evolution of, and revolution in, land surface schemes designed for climate models. *Int. J. Climatol.,* **23,** 479–510.

Pielke, R. A., Sr., 2001: Influence of the spatial distribution of vegetation and soils on the prediction of cumulus convective rainfall. *Rev. Geophys.,* **39,** 151–177.

Pinzón, J. E., 2002: Using HHT to successfully uncouple seasonal and interannual components in remotely sensed data. *Proc. Sixth World Multiconf. on Systematics, Cybernetics and Informatics (SCI2002),* Orlando, FL, International Institute of Informatics and Systemics, 287–292.

Pinzón, J. M., M. Brown, and C. J. Tucker, 2004: Satellite time series correction of orbital drift artifacts using empirical model decomposition. *Hilbert–Huang Transform: Introduction and Applications,* N. Huang, N. E. Huang, and S. S. P. Shen, Eds., World Scientific, 285–295.

Rajagopalan, B., M. E. Mann, and U. Lall, 1998: A multivariate frequency domain approach to long-lead climate forecasting. *Wea. Forecasting,* **13,** 58–74.

Ropelewski, C. F., and M. S. Halpert, 1986: North American precipitation and temperature patterns associated with the El Niño/Southern Oscillation (ENSO). *Mon. Wea. Rev.,* **114,** 2352–2362.

Salvucci, G. D., J. A. Saleem, and R. Kaufman, 2002: Investigating soil moisture feedbacks on precipitation with tests of Granger causality. *Adv. Water Resour.,* **25,** 1305–1312.

Schonauer, K. T., 2007: Temporal evolution of hydrological and meteorological drought indicators for select basins in Arizona. M.S. thesis, School of Natural Resources, University of Arizona, 105 pp.

Schubert, S. D., M. J. Suarez, P. J. Pegion, M. A. Kistler, and A. Kumar, 2002: Predictability of zonal means during boreal summer. *J. Climate,* **15,** 420–434.

——, ——, ——, R. D. Koster, and J. T. Bacmeister, 2004: Causes of long-term drought in the U.S. Great Plains. *J. Climate,* **17,** 485–503.

Seager, R., Y. Kushnir, C. Herweijer, N. Naik, and J. Velez, 2005: Modeling of tropical forcing of persistent droughts and pluvials over western North America: 1856–2000. *J. Climate,* **18,** 4065–4088.

Small, E. E., 2001: The influence of soil moisture anomalies on variability of the North American monsoon system. *Geophys. Res. Lett.,* **28,** 139–142.

Stahle, D. W., and Coauthors, 2009: Cool- and warm-season precipitation reconstructions over western New Mexico. *J. Climate,* **22,** 3729–3750.

Tucker, C. J., J. E. Pinzón, M. E. Brown, D. Slayback, E. W. W. Pak, R. Mahoney, E. Vermote, and N. El Saleous, 2005: An extended AVHRR 8-km NDVI data set compatible with MODIS and SPOT vegetation NDVI Data. *Int. J. Remote Sens.,* **26,** 4485–4498.

Watts, C. J., R. L. Scott, J. Garatuza-Payan, J. C. Rodriguez, J. H. Prueger, W. P. Kustas, and M. Douglas, 2007: Changes in vegetation condition and surface fluxes during NAME 2004. *J. Climate,* **20,** 1810–1820.

Wei, J., R. E. Dickinson, and H. Chen, 2008: A negative soil moisture–precipitation relationship and its causes. *J. Hydrometeor.,* **9,** 1364–1376.

Zhang, Z., and M. E. Mann, 2005: Coupled patterns of spatiotemporal variability in Northern Hemisphere sea level pressure and conterminous U.S. drought. *J. Geophys. Res.,* **110,** D03108, doi:10.1029/2004JD004896.